

ON THE INTERACTION BETWEEN DIFFERENTIAL ROTATION AND MAGNETIC FIELDS IN THE SUN

ALLAN SACHA BRUN

*DSM/DAPNIA/SaP, CEA Saclay, 91191 Gif-sur-Yvette Cedex, France;
e-mail sacha.brun@cea.fr*

(Received 1 December 2003; accepted 30 December 2003)

Abstract. We have performed 3-D numerical simulations of compressible convection under the influence of rotation and magnetic fields in spherical shells. They aim at understanding the subtle coupling between convection, rotation and magnetic fields in the solar convection zone. We show that as the magnetic Reynolds number is increased in the simulations, the magnetic energy saturates via nonlinear dynamo action, to a value smaller but comparable to the kinetic energy contained in the shell, leading to increasingly strong Maxwell stresses that tend to weaken the differential rotation driven by the convection. These simulations also indicate that the mean toroidal and poloidal magnetic fields are small compared to their fluctuating counterparts, most of the magnetic energy being contained in the non-axisymmetric fields. The intermittent nature of the magnetic fields generated by such a turbulent convective dynamo confirms that in the Sun the large-scale ordered dynamo responsible for the 22-year cycle of activity can hardly be located in the solar convective envelope.

1. Introduction

Observations of the solar convective surface reveal that it rotates differentially, the equatorial regions being about 30% faster than the polar regions. Thanks to helioseismology, it has been demonstrated that this strong differential rotation imprints the whole convective envelope to then become uniform in the radiative interior (Thompson *et al.*, 2003; Couvidat *et al.*, 2003). This transition occurs at the base of the convection zone ($r \simeq 0.71 R_{\odot}$, where R_{\odot} is the solar radius) in a thin shear layer called the tachocline. The Sun also exhibits both random and cyclic magnetic activity with phenomena as diverse as coronal mass ejections, prominences and sunspots (Stix, 2002). Understanding the physical processes behind such a complex magnetohydrodynamical (MHD) system and how they are interacting to yield ordered properties such as the large-scale mean flows or the 22-year cycle, has turned out to be one of the major challenges of modern astrophysics (Brummel, Cataneo, and Toomre, 1995; Ossendrijver, 2003). Indeed such intricate nonlinear interactions can not be directly predicted from first principles. Therefore alternative techniques have been developed to improve our ‘physical intuition’ about the working of such complex dynamical processes. For example, mean field theory (Moffat, 1978; Krause and Rädler, 1980) has been successful at laying down the basic principles behind the solar dynamo, such as the ω and α effects. More



recently, fully nonlinear 3-D MHD simulations have started to refine and to improve our understanding. It is currently believed that our star operates a dynamo at two differing ranges of spatial and temporal scales (Cattaneo and Hughes, 2001). The global dynamo yielding the regular 22-year cycle and butterfly diagrams for sunspot emergence is likely to be seated within the tachocline (Parker, 1993). The origin of the rapidly varying and smaller scale magnetism is probably due to local dynamo action.

We would like here to address some aspects of the nonlinear coupling between convection, rotation and magnetic fields in the Sun. We believe that numerical simulations of a rotating conducting convective fluid in full spherical geometry could help understanding of this difficult problem. Unfortunately even today 3-D simulations of the whole solar dynamo problem are intractable considering the 6 orders of spatial and temporal scales realized in the turbulent solar convection zone. As an alternative one can split the dynamo problem into ‘blocks’ that answer specific questions, such as magnetic field amplification, magnetic field pumping, flux tube rising . . . Following the pioneering work of Gilman and Glatzmaier (Gilman, 1983; Glatzmaier, 1987), we have conducted global, high-resolution (up to spherical harmonic degree $\ell_{\max} = 340$), 3-D MHD simulations of the bulk of the solar convection zone. Since both the α and ω effects are thought to play a crucial role in the working of the solar dynamo, we are interested in studying the interplay between differential rotation and magnetic fields and how dynamo generated magnetic fields feedback on the large scale convection via Lorentz forces. In particular we would like to address the following two questions: (a) Are there numerical solutions that both display a dynamo generated magnetic field and retain a strong differential rotation profiles as deduced by helioseismic inversions? (b) What are the respective roles of the Reynolds and Maxwell stresses and of the large-scale magnetic torque in the transport of the angular momentum in our turbulent convective rotating shells?

We briefly present in Section 2 our numerical model and the anelastic spherical harmonics (ASH) code used in this work. In Section 3 we discuss the influence of magnetic fields on the turbulent rotating convective zone, compare our results with past and present observations of the Sun and with earlier 3-D MHD numerical simulations of the solar convection envelope. We then summarize in Section 4 our findings.

2. Formulating the Problem

The ASH code solves the 3-D MHD anelastic equations of motion in a rotating spherical shell geometry using a pseudo spectral semi-implicit method (Clune *et al.*, 1999; Brun, Miesch, and Toomre, 2004). The anelastic approximation captures the effects of density stratification without having to resolve sound waves which would severely limit the time steps. The resulting equations are fully non-

linear in velocity and magnetic field variables; the thermodynamic variables are separated with respect to a spherically symmetric and evolving mean state (denoted with an overbar) and fluctuations about this mean state:

$$\nabla \cdot (\bar{\rho} \mathbf{v}) = 0, \quad (1)$$

$$\begin{aligned} \bar{\rho} \left(\frac{\partial \mathbf{v}}{\partial t} + (\mathbf{v} \cdot \nabla) \mathbf{v} + 2\Omega_{\mathbf{o}} \times \mathbf{v} \right) = & -\nabla P + \rho \mathbf{g} + \frac{1}{4\pi} (\nabla \times \mathbf{B}) \times \mathbf{B} - \\ & -\nabla \cdot \mathcal{D} - [\nabla \bar{P} - \bar{\rho} \mathbf{g}], \end{aligned} \quad (2)$$

$$\begin{aligned} \bar{\rho} \bar{T} \frac{\partial S}{\partial t} + \bar{\rho} \bar{T} \mathbf{v} \cdot \nabla (\bar{S} + S) = & \nabla \cdot [\kappa_r \bar{\rho} c_p \nabla (\bar{T} + T) + \kappa \bar{\rho} \bar{T} \nabla (\bar{S} + S)] + \\ & + \frac{\eta}{4\pi} (\nabla \times \mathbf{B})^2 + 2\bar{\rho} \nu [e_{ij} e_{ij} - 1/3 (\nabla \cdot \mathbf{v})^2], \end{aligned} \quad (3)$$

$$\frac{\partial \mathbf{B}}{\partial t} = \nabla \times (\mathbf{v} \times \mathbf{B}) - \nabla \times (\eta \nabla \times \mathbf{B}), \quad (4)$$

where $\mathbf{v} = (v_r, v_\theta, v_\phi)$ is the local velocity in spherical coordinates in the frame rotating at constant angular velocity $\Omega_{\mathbf{o}} = \Omega_o \mathbf{e}_z$, \mathbf{B} is the magnetic field, κ_r is the radiative diffusivity, η is the effective magnetic diffusivity, ν and κ are effective eddy diffusivities, \mathcal{D} is the viscous stress tensor and e_{ij} is the strain rate tensor. All the other variables have their usual meaning.

We use a toroidal and poloidal decomposition that enforces the mass flux and the magnetic fields to remain divergence free. The effects of the steep entropy gradient close to the surface has been softened by introducing a subgrid scale (SGS) transport of heat to account for the unresolved motions, and enhanced diffusivities are used in these large eddy simulations (LES). The boundary conditions at the top and bottom of the computational domain are stress-free impenetrable walls for the velocity field, constant entropy gradient for the entropy and match to a potential field for the magnetic field.

The model is a simplified description of the solar convection zone: solar values are taken for the heat flux, rotation rate, mass and radius, and a perfect gas is assumed. The computational domain extends from $0.72 R_\odot$ to $0.96 R_\odot$, thereby concentrating on the bulk of the unstable zone and here not dealing with penetration into the radiative interior nor with the partially ionized surface layers. The maximum numerical resolution used in case *M3* is $N_r = 129$ radial collocation points and $N_\theta = 512$ and $N_\phi = 1024$ latitudinal and longitudinal grid points (corresponding to taking all degrees up to the spherical harmonic degree $\ell_{\max} = 340$). The typical density difference across the shell in radius is about 30.

We start our MHD simulations from an already evolved and equilibrated purely hydrodynamical solution, namely case *H*, characterized by a Rayleigh number $Ra = 10^5$, a Taylor number $Ta = 1.2 \times 10^6$ and a Prandtl number $Pr = 1/8$. This case possesses a strong, almost solar-like differential rotation (cf. Figure 3

and Brun, Miesch, and Toomre, 2004). A seed axisymmetric dipolar magnetic field is then introduced in the convective spherical shell and the simulations evolved in time.

In the following section we report on the main results obtained with our numerical simulations by comparing two magnetic cases, $M1$ and $M3$, among many others that we have computed. These two cases possess in turn a magnetic Prandtl number $P_m = \nu/\eta$ of 2 and 4, leading in case $M3$ to a rms magnetic Reynolds number ($R_m = \tilde{v}L/\eta$, where L is the shell thickness and \tilde{v} a representative rms velocity), about a factor of two bigger than in case $M1$. Both simulations have been started with a magnetic energy (ME) seven order of magnitude smaller than the total kinetic energy (KE) contained in the non-magnetic convective case H (i.e., $(ME/KE)_0 = 10^{-7}$).

3. Rotating Convective Zone and Associated Mean Flows in the Presence of Magnetic Fields

The interaction between differential rotation and magnetic fields is complex and nonlinear; the differential rotation amplifies the mean toroidal magnetic field via the ω -effect and the Lorentz forces feedback on the flow as soon as the mean or fluctuating magnetic fields reach a threshold amplitude. We have found in the numerical experiments presented here that the magnetic fields do have a strong influence on the resulting mean flows achieved in convective spherical shells but not exactly in the way anticipated by mean field theory.

3.1. KINETIC AND MAGNETIC ENERGY DISTRIBUTIONS

Let us first consider the energy budget in our simulations as we break down the kinetic and magnetic energies into axisymmetric and non-axisymmetric parts. In Figure 1 we display the time trace of the kinetic and magnetic energies of $M1$ and $M3$ over respectively 1200 and 4000 days (corresponding in each case to several ohmic decay times $\tau_\eta = \tilde{v}L/(\pi^2\eta)$). We see that the magnetic energy of case $M1$ (hereafter ME1) is decaying whereas that in case $M3$ (ME3) has grown by more than a factor of 10^5 , reaching a value of 7% of the kinetic energy (KE3). This clearly indicates that case $M3$ is running an efficient dynamo. The exponential growth of ME3 at the beginning of the temporal evolution (first 600 days) and its subsequent nonlinear saturation, due to the feedback from the Lorentz forces, are typical of dynamo action and are in good agreement with the expected properties of a stellar dynamo (cf., Cattaneo, Hughes, and Weiss, 1991). The rise of ME3 leads to a decrease of KE3 (by 37%), but does not totally compensate for that reduction. We found that the sum of KE3+ME3 is smaller than the initial kinetic energy KE0 contained in case H , indicating that the energy redistribution in our convective shells is modified by the presence of magnetic fields. To assess the cause of the

large reduction of KE3, we also display in Figure 1 the kinetic energy contained in the differential rotation (DRKE3) and in the convective motions (CKE3) (that in the meridional circulation is only $\sim 0.3\%$ of KE3). It is clear that DRKE3 is more affected by the presence of magnetic energy than CKE3, becoming even smaller than CKE3 after 3800 days. This result suggests that the decrease in kinetic energy is due to a weakening of the energy contained in the differential rotation rather than in a less vigorous convection. In case *M3*, ME is found to be equal or above local equipartition near the top of the domain, for about 2% of the surface area. The radial distribution of ME3 peaks near the bottom of the shell. This is certainly due to magnetic pumping by the strongest downflows or plumes (Tobias *et al.*, 2001).

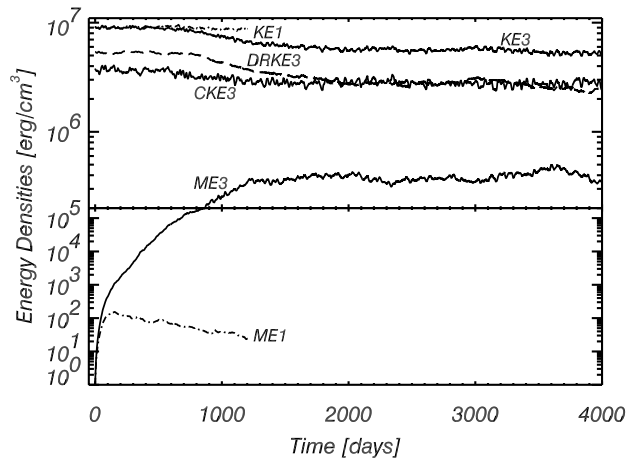


Figure 1. Temporal evolution of the kinetic energy (KE) and magnetic energy (ME) for cases *M1* and *M3*, involving respectively rms magnetic Reynolds numbers R_m of 250 and 500.

The mean toroidal and poloidal magnetic energies (TME and PME) contribute respectively only 1.5% and 0.5% of ME3. The non-axisymmetric magnetic fields thus contained 98% of the total magnetic energy. In the Sun, the mean toroidal field is about 2 orders of magnitude larger than the mean poloidal field. The fact that in our simulation of global-scale convection this ratio is of order 1, indicates that the Sun must generate the strong large scale mean toroidal field outside its convective zone. The stably stratified tachocline at the base of the solar convection zone seems a natural location to amplify even further the mean toroidal field to the required observational level. Pumping of the magnetic field by turbulent convective plumes could certainly help in continuously supplying the tachocline with fields produced in the solar envelope.

When comparing the energy redistribution achieved in our simulations with that found in the earlier numerical simulations of the solar convective envelope by Gilman (1983), using the Boussinesq approximation, and by Glatzmaier (1987) using the anelastic approximation, we find a good overall agreement. For instance,

we all find that the larger is the magnetic energy contained in the convective shell, the smaller is DRKE, resulting in a damping of the differential rotation (cf., Section 3.3). We also find that increasing the magnetic Prandtl number P_m , leads to a larger amplitude of the magnetic energy. The main differences are found in the relative amplitude of the mean toroidal and poloidal magnetic energies achieved in the simulations. We have seen that TME and PME in case *M3* are rather small compared to both ME and KE. In the work of Glatzmaier, ME is only about 0.1% of KE, so being relatively much smaller than in case *M3*, but TME represents 85% of that total. This is certainly due to the presence in these simulations of a stable region at the bottom of the convective envelope. In the work of Gilman discussing several cases, there is one case that possesses a ratio ME/KE of about 7% as in case *M3* (case with $Q = \eta/\kappa = 1.7$), but TME and PME are again found to be a significant fraction of ME ($\sim 20\%$). The case with $Q = 0.5$ possesses a small mean magnetic energy $TME + PME \sim 3.5\%$, closer to that found in case *M3*, but its magnetic energy rose to 45% of KE. At that level of magnetism the kinetic energy contained in the differential rotation (DRKE) drops to only 30% of KE, resulting in an excessively weak differential rotation. Such strong damping of the angular velocity is not observed in case *M3* (cf. Section 3.3). Certainly the different sets of parameters (Ra , Ta , Pr , and P_m) used in their simulations by the three authors, explain for the most part the differences seen in the energy ratios, making a direct quantitative comparison rather difficult. Another explanation could be the numerical resolution used in the simulations, since in our study it is more than 10 times larger (e.g., $\ell_{\max} = 340$ vs $\ell_{\max} = 24$ or 32 in the earlier studies). We indeed find that the magnetic energy spectrum in case *M3* (not shown) does not peak at the azimuthal wavenumber $m = 0$ as in the cases published by Gilman (1983), but between $m = 1$ and 10 , confirming the non-axisymmetric nature of the magnetic fields.

3.2. MORPHOLOGY OF THE VELOCITY AND MAGNETIC FIELDS

The convection realized in cases *H*, *M1* and *M3* is intricate and time dependent, involving continuous shearing, cleaving and merging of the convective cells. Figure 2 displays for case *M3* the radial, latitudinal and longitudinal components of both the velocity and magnetic fields near the top of the domain at one instant in time.

We note that the radial velocity (top left panel) is asymmetric, downflows being concentrated in narrow lanes surrounding the broad upflows. Pronounced vortical structures are evident at the interstices of the downflows network. They are cyclonic, i.e., counterclockwise in the northern hemisphere and clockwise in the southern one. The strongest of these vortex tubes or ‘plumes’ extend through the whole domain depth. These plumes represent coherent structures that are surrounded by more chaotic flows. They tend to align with the rotation axis and to be tilted away from the meridional planes, leading to Reynolds stresses that are crucial ingredi-

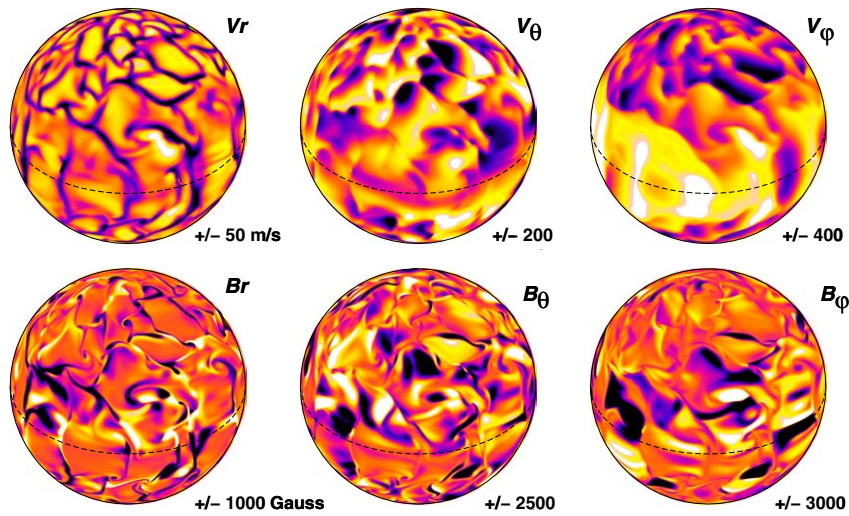


Figure 2. Snapshot of the radial, latitudinal and longitudinal velocities (*upper row*) and magnetic fields (*lower row*) in case *M3* near the top ($0.96 R_{\odot}$) of the spherical domain. Downflows and negative polarity appear dark. Representative min/max amplitudes for the velocities (in m s^{-1}) and for the magnetic fields (in gauss) are indicated at the bottom right of each panel. The *dashed curve* delineates the equator.

ents in redistributing the angular momentum within the shell (cf., Section 3.3). The latitudinal velocity v_{θ} is more patchy and symmetric than v_r . The horizontal velocity v_{ϕ} possesses the clear banded signature of the differential rotation driven by the convection with a fast/prograde equator and slow/retrograde high latitude regions. The strongest downflow lanes are apparent in the horizontal velocities.

Turning now to the bottom row of Figure 2, we notice that the magnetic fields possess a finer structure than the velocity fields (due to our choice of $P_m > 1$), and that the radial and horizontal components of the magnetic fields possess different morphologies. The radial magnetic field has been swept into the downflow lanes. This is not the case for the horizontal fields, where large patches of a given polarity are found in the middle of the convective cells. Strong magnetic field gradients are present near the downflows network, where the magnetic fields are continuously sheared and stretched. Substantial magnetic helicity is present, involving complex winding of the toroidal magnetic fields along their length, with both polarities interchanging their position into intricate structures. There are no obvious correlations between the two horizontal vector fields. By contrast the strongest (unsigned) radial magnetic field $|B_r|$ does correlate with the strongest downflow lanes seen in the radial velocity. In all the six fields displayed, a clear north–south asymmetry is present.

3.3. DIFFERENTIAL ROTATION WITH OR WITHOUT MAGNETIC FIELDS

Figure 3 (left panel) shows the sidereal angular velocity $\Omega(r, \theta)$ of case *H* (converted into nHz, with $\Omega_o/2\pi = 414$ nHz). There is a strong rotational contrast $\Delta\Omega$ between the fast equator and the slow high-latitude regions. The contrast $\Delta\Omega$ from 0° to 60° is 140 nHz equivalent to a $\Delta\Omega/\Omega_o$ of about 34%. There is some constancy along radial lines at mid latitudes (45° – 75°) and a systematic decrease of Ω with latitude even in the polar regions. The angular velocity profile is in good qualitative agreement with helioseismic inversions of the solar differential rotation (Thompson *et al.*, 2003). The differential rotation profile in case *H* is due to the equatorward transport of angular momentum by Reynolds stresses, themselves closely related to the tilted plumes realized in turbulent convective flows which are the source of velocity correlations such as $\widehat{v'_r v'_\phi}$. These Reynolds stresses oppose the poleward transport of angular momentum by viscous stresses and meridional circulation and lead to an equatorial acceleration (Brun and Toomre, 2002).

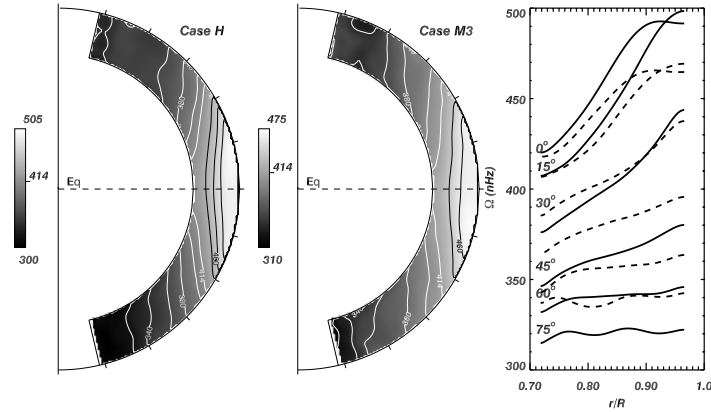


Figure 3. Temporal and longitudinal averages of the angular velocity profiles achieved in case *H* and *M3* over an interval of 100 days (shown as contour plots). These cases exhibit a prograde equatorial rotation and a strong contrast $\Delta\Omega$ from equator to pole, as well as possess a high-latitude region of particularly slow rotation. In the right panel, displaying radial cuts of Ω at indicated latitudes for both cases, the reduction in $\Delta\Omega$ due to the nonlinear feedback of the Lorentz forces (solid vs dashed lines) can be assessed.

In Figure 3 (middle panel) we display the Ω profile achieved in case *M3*. Case *M1* possesses a differential rotation identical to case *H* and is not shown. With fairly strong magnetic fields sustained within the bulk of the convection zone in case *M3*, it is to be expected that the differential rotation Ω will respond to the feedback from the Lorentz forces. As seen in Section 3.1 the main effect of the Lorentz forces is to extract energy from the kinetic energy stored in the differential rotation. As a consequence $\Delta\Omega/\Omega_o$ drops by $\sim 30\%$ in going from 34% in case *H* down to 24% in case *M3*. This value is thus even closer to the value of 22%

(between 0° and 60° of latitude) inferred from seismic inversion of the solar profile (Thompson *et al.*, 2003). Since the convection is still able to maintain an almost solar-like angular velocity contrast from low-to-high latitudes, the magnetic field does not reduce the differential rotation as much as one might expect. One possible explanation for such a mild reduction of the differential rotation contrast could be the fact that ME is only 7% of KE. In Section 3.1 we have shown that a rather high level of magnetism is needed to damp the differential rotation significantly (around a ratio of ME/KE of about 0.25, see also Gilman, 1983). The fact that in case *M3* the mean poloidal magnetic field is weak compared to its fluctuating counterpart, indicates that the slowing down of the differential rotation is not due to the torque applied by the large-scale axisymmetric magnetic fields but to a more subtle effect connected to the twisted structure of the magnetic fields.

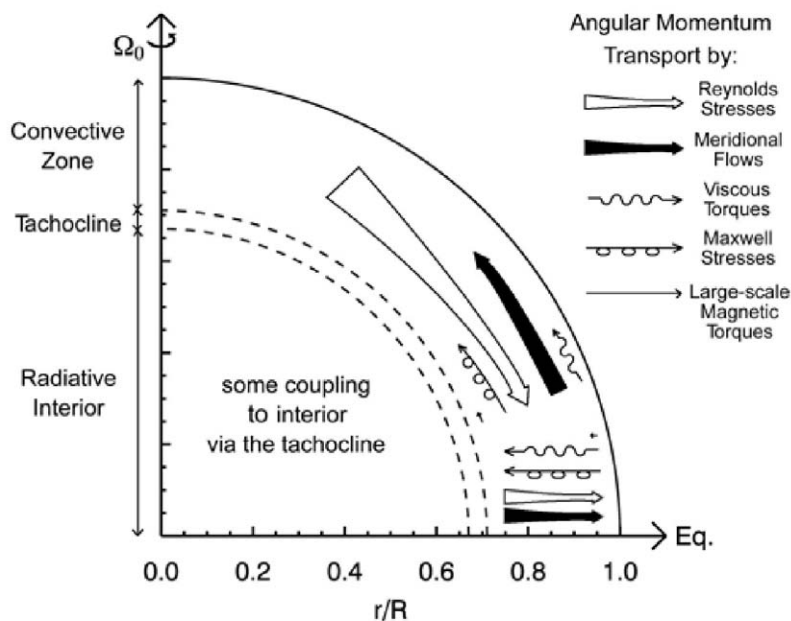


Figure 4. Illustration of the balance of angular momentum in latitude and radius in case *M3* between the Reynolds stresses, Maxwell stresses, viscous torques, large-scale magnetic torques and the meridional circulation. The arrow length is proportional to the amplitude of the process.

A careful study of the redistribution of the angular momentum in our shell reveals that the source of the reduction of the latitudinal contrast of Ω can be attributed to the poleward transport of angular momentum by the Maxwell stresses (cf. Figure 4, and Brun *et al.*, 2004 for more details). The large-scale magnetic torques are found to be 2 orders of magnitude smaller, confirming the small dynamical role played by the mean fields in our simulations. The Reynolds stresses now need to balance the angular momentum transport by the meridional circulation, the viscous

diffusion and the Maxwell stresses. This results in a less efficient speeding up of the equatorial regions. However, the Maxwell stresses are not yet the main players in redistributing the angular momentum and case *M3* is able to sustain a strong differential rotation as observed in the present Sun. There is good agreement between this work and the earlier studies of Gilman (1983) and Glatzmaier (1987) on the role of the Maxwell and Reynolds stresses in redistributing the angular momentum in the shell. We all find that the magnetic fields tend to make the rotation profile more uniform. Our results differ on the actual strength of such reduction and on the profile of angular velocity achieved.

Based on observations of the Sun by J. Hevelius in 1642–1644, Eddy, Gilman, and Trotter (1976) showed that during this period, the few observed solar sunspots in the equatorial regions were rotating about 4% faster than today. We believe that the fact that case *M1* (or equivalently case *H*) is rotating faster than case *M3* (because of the absence of substantial magnetic stresses acting to slow down the equatorial regions and speed up the poles), has some bearing on Eddy, Gilman, and Trotter's results. Certainly a reduced level of magnetism in a convective zone could lead to faster equatorial region and slower polar regions, i.e., to a larger differential rotation contrast. It is not clear if during the Maunder minimum only the large-scale dynamo action seated in the tachocline was reduced in amplitude (explaining the fewer number of observed sunspots), or if the small scale dynamo action generated by the turbulent convective motions was weaker as well. Let's assume here that both dynamos were weaker in the Sun during the Maunder minimum, and that reduced/weaker Maxwell stresses (and/or large-scale magnetic torques) resulted in a faster equatorial region, in a way similar to what is realized in cases *H* or *M1*. We can then use our simulated Ω profile to deduce the latitudinal distribution of the change in Ω with or without the feedback of strong magnetic fields. We found that such a function of θ (the colatitude) varies from about -6% ($\theta = 0$) to about $+6\%$ ($\theta = 90^\circ$) in comparing cases *H* and *M3*. If we now apply this scaling function to the present surface differential rotation, here approximated as $\Omega_\odot(\theta) = 456 - 72 \times \cos^2(\theta) - 42 \times \cos^4(\theta)$, we can extrapolate the solar differential rotation profile to a period of 'grand activity minimum'.

Figure 5 displays the current, mid-1600s and extrapolated Ω profiles (the old profile being limited to the $\pm 20^\circ$ band, cf. Figures 3 and 4 of Eddy, Gilman, and Trotter, 1976). The agreement between the extrapolated curve and the old data points is reasonable, and corresponds to a faster rotation by about 4 to 5% at the equator. In Eddy, Gilman, and Trotter the old and present rotational curves meet at a latitude of about $\pm 20^\circ$, whereas in the extrapolated rotation curve it occurs at 30° . Beyond this latitude of 30° , the extrapolated rotational curve predicts that these regions were likely rotating slower than today.

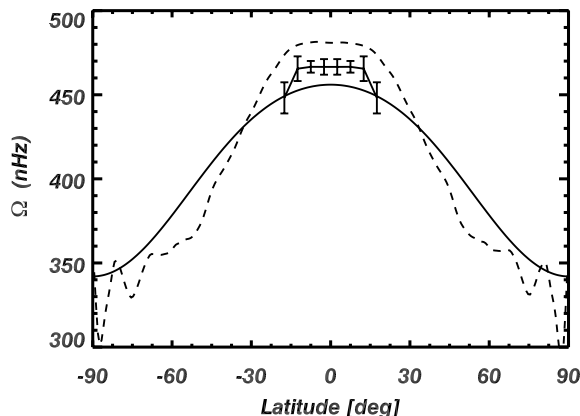


Figure 5. Possible surface differential rotation profile of the Sun during the quiet magnetic phase of the Maunder minimum. The current solar profile is shown in plain solid and the modified profile (*dashed line*) is deduced after multiplying the solid line by the scaling law $(\Omega_{surf-H}(\theta) - \Omega_{surf-M3}(\theta))/\Omega_{surf-H}(\theta)$. The *solid line* superimposed with $1-\sigma$ error bars, reproduces the results of Eddy *et al.* (1976) during the 1642-1644 period. In the $\pm 20^\circ$ latitudinal band the agreement between the extrapolated curve and Eddy *et al.* study is reasonable.

4. Conclusions

Our 3-D MHD simulations of convection in deep spherical shells, achieved through the use of massively parallel supercomputers, are showing how the strong differential rotation present in the Sun may be maintained through fairly complex redistribution of angular momentum by the turbulent compressible flows in a conducting media. We have studied the interaction of convection and rotation with seed magnetic fields in such shells, and found solutions in which sustained magnetic dynamo action can be realized without unduly reducing the angular velocity contrasts maintained by the convection, thus answering positively question (a) raised in the Introduction. In seeking to answer question (b), we have found that the Maxwell stresses oppose the Reynolds stresses and seek to speed up the poles and that the large-scale magnetic torques play almost no role. The reduction in differential rotation is thus not due to the torque applied by the large-scale axisymmetric (i.e., $m = 0$) magnetic fields but to a more subtle braking effect exerted by the non-axisymmetric magnetic fields. In our models, the stronger are the dynamo generated fields, the weaker is the differential rotation, confirming the earlier results of Gilman (1983) and Glatzmaier (1987). We find that above a ratio of magnetic to kinetic energy of about 0.25, the differential rotation becomes excessively damped. It seems that a ratio of ME/KE of about 0.05–0.07 leads to a reduction of the differential rotation compatible with that seen in the Sun when comparing past and present observations (cf., Section 3.3). In the context of a mean field solar dynamo, our results imply that the ω -effect is likely 'quenched' more strongly than the ' α '-

effect by the presence of magnetic fields. But the fibril and intermittent nature of the dynamo generated magnetic fields seen in our simulations casts some doubts on the ability of mean field dynamo concepts to truly capture the intricate interplay between convection, rotation and magnetic fields. Our simulations of large-scale convection in spherical geometry strengthen the current paradigm that the strong mean toroidal magnetic field at the origin of the surface sunspots is likely stored and amplified in the tachocline at the base of the solar convective zone. The role of the convective envelope being to continuously produce, pump down and supply the disorganized magnetic fields to the tachocline. We are aware that the numerical experiments discussed in this work represent at best a crude description of the solar dynamics and that great care has to be taken in extending their results to the Sun. In reality the Sun is much more complex with the presence of strong shear layers both at the bottom and at the top of its convective zone and the possibility to globally reorganize its magnetic field and helicity via intense coronal mass ejections. We intend to address some of these issues in forthcoming papers.

Acknowledgements

The author is grateful to J. J. Aly, M. S. Miesch, J. Toomre, S. Turck-Chièze and J.-P. Zahn for enlightening discussions and to the anonymous referee for his constructive comments. The simulations with ASH were carried out with NSF NPACI support to various American supercomputer centers and within CCRT at CEA.

References

- Brummell, N. H., Cattaneo, F., and Toomre, J.: 1995, *Science* **269**, 1370.
 Brun, A. S. and Toomre, J.: 2002, *Astrophys. J.* **570**, 865.
 Brun, A. S., Miesch, M., and Toomre, J.: 2004, *Astrophys. J.*, submitted.
 Cattaneo, F. and Hughes, D. W.: 2001, *Astron. Geophys.* **42**, 18.
 Cattaneo, F., Hughes, D. W., and Weiss, N. O.: 1991, *Monthly Notices Royal Astron. Soc.* **253**, 479.
 Clune, T. L., Elliott, J. R., Glatzmaier, G. A., Miesch, M. S., and Toomre, J.: 1999, *Parallel Comput.* **25**, 361.
 Couvidat, S., Garcia, R. A., Turck-Chièze, S., Corbard, T., Henney, C. J. and Jimenez-Reyes, S.: 2003, *Astrophys. J.* **597**, L77.
 Eddy, J. A., Gilman, P. A., and Trotter, D. E.: 1976, *Solar Phys.* **46**, 3.
 Gilman, P. A.: 1983, *Astrophys. J.* **53**, 243.
 Glatzmaier, G. A.: 1987, in *The Internal Solar Angular Velocity*, B. R. Durney and S. Sofia (eds.), D. Reidel, Dordrecht, p. 263.
 Krause, F. and Rädler, K. H.: 1980, *Mean Field Magnetohydrodynamics and Dynamo Theory*, Pergamon, Oxford.
 Moffat, H. K.: 1978, *Magnetic Field Generation in Electrically Conducting Fluids*, Cambridge University, Cambridge.
 Ossendrijver, M.: 2003, *Astron. Astrophys. Rev.* **11**, 287.
 Parker, E. N.: 1993, *Astrophys. J.* **408**, 707.

Stix, M.: 2002, *The Sun, an Introduction*, 2nd edition, Springer, Berlin.

Thompson, M. J., Christensen-Dalsgaard, J., Miesch, M. S., and Toomre, J.: 2003, *Ann. Rev. Astron. Astrophys.* **41**, 599.

Tobias, S. M., Brummell, N. H., Clune, T. L., and Toomre, J.: 2001, *Astrophys. J.* **549**, 1183.